THESIS FOR THE DEGREE OF LICENTIATE OF ENGINEERING IN MACHINE AND VEHICLE SYSTEMS

Analysis of the Base Wake on Passenger Vehicles

LENNERT STERKEN

Department of Applied Mechanics
CHALMERS UNIVERSITY OF TECHNOLOGY

Göteborg, Sweden 2013

Analysis of the Base Wake on Passenger Vehicles
LENNERT STERKEN

Thesis for the degree of Licentiate of Engineering 2013:14
ISSN 1652-8565
Department of Applied Mechanics
Chalmers University of Technology
SE-412 96 Göteborg
Sweden
Telephone: +46 (0)31-772 1000

Chalmers Reproservice
Göteborg, Sweden 2013

Analysis of the Base Wake on Passenger Vehicles
Thesis for the degree of Licentiate of Engineering in Machine and Vehicle Systems
LENNERT STERKEN
Department of Applied Mechanics
Chalmers University of Technology

Abstract

Car manufacturers are presented by a continuous increase in fuel prices and by ever more strict legislations regarding CO_2-emissions. Decreasing the driving resistance and hence the fuel consumption of their vehicles helps to improve their market share. Aerodynamics plays an important role since it is a significant contributor to the driving resistance at typical driving speeds of 70 km/h and above.

Passenger vehicles are defined as bluff bodies of which the main source of air resistance is pressure drag. This drag is caused by the wake a car creates and can be explained by the pressure difference between the front and the rear of the vehicle. Therefore, understanding the behaviour of the wake in time and in space is crucial in order to accomplish the goal of drag reduction.

Experimental and numerical investigations have been conducted on a 2WD and 4WD Volvo XC60 to study the effects of geometrical changes to the base pressure and wake shape of the car. Surface pressure measurement equipment and two omni-directional pressure probes were used for the base and wake measurements, respectively. Results show a base pressure reduction with an increased standard deviation for a reduction in drag caused by covering the upper and lower front grille. In the flow field this effect is visible as a smaller wake size and high-energy underbody flow enhancing the total pressure recovery in the far wake. Improved energy recovery in the far wake can also be realised by having an extended roof spoiler, that causes a delayed separation and a more downward inclination of the shear layer.
The corresponding numerical simulations in general show good agreement with the experiments in force trend predictions. The configuration changes have a similar flow field effect in CFD compared to the wind tunnel. However some significant differences in wake shape behind the vehicle can also be observed.

A new visualisation technique has been developed to differentiate the contribution of the different geometrical sections of the car to the overall air resistance. This creates the opportunity to quantify the drag of each section in relation to the total drag of the vehicle.

Keywords: External aerodynamics, Wake, Wind tunnel, CFD, Pressure measurements, Local drag

Acknowledgements

This research could only be accomplished thanks to the supervision and guidance of numerous people. Through this way I would like to take the opportunity to acknowledge them.

Firstly, I would like to thank my supervisors at Volvo Car Corporation, Dr. Simone Sebben and Tim Walker, for giving me a chance to return to Göteborg after a few years of absence and start my PhD studies. Their continuous guidance, support and suggestions gave me inspiration to fulfil my goals. I also would like to thank Dr. Christoffer Landström to assist me in finding a way in the complex web of being a Phd student. A special thanks goes to my examiner Professor Lennart Löfdahl at Chalmers University of Technology for giving me the opportunity to conduct my research under his department.

To my manager, Dr Jonas Ask, and Dr. Dragos Moroianu for the more fundamental numerical questions I could address. I would also like to thank all my colleagues at the 91780 group for the great working atmosphere and the regular social activities to enhance our *CFD familje* feeling.
In addition, I would like to send my gratitude to my colleagues at the 91760 section, and in special Tom Lindén with the experimental setup and Linda Josefsson for assisting me with the MWT and the PSI system.

To Bo Antonsson, Stefan Gribling and all workshop technicians, without their preparations no car would have reached the wind tunnel.

At Chalmers University of Technology I would like to thank my fellow PhD students: Alexey Vdovin and Teddy Hobeika for their interesting discussions and support throughout this thesis. Furthermore I would like to acknowledge all department members with a special thanks to Andrew Dawkes for reviewing this thesis.

I would also like to acknowledge VINNOVA/FFI for funding this project without whom this project would not have occurred.

Finally I would like to thank my family and friend, and in special my parents for all the years supporting me to accomplish my dreams and give me all the possibilities to extend my knowledge and experiences.

Nomenclature

A	Frontal area	$[m^2]$
f_r	Rolling resistance coefficient	[-]
C_D	Drag coefficient	[-]
$C_{D_{wake}}$	Local drag coefficient	[-]
C_D^*	Local drag coefficient on polar mesh	[-]
C_L	Lift coefficient	[-]
C_p	Pressure coefficient	[-]
$C_{p_{tot}}$	Total pressure coefficient	[-]
F_A	Driving resistance due to acceleration	[N]
F_D	Aerodynamic driving resistance	[N]
F_G	Driving resistance due to gravity	[N]
F_R	Rolling resistance	[N]
S	Wake plane area	$[m^2]$
V	Velocity	$[m/s]$
V_x, V_y, V_z	Velocity components	$[m/s]$
V_∞	Free stream velocity	$[m/s]$
α	Road inclination angle	[-]
ρ	Air density	$[kg/m^3]$

Abbreviations

2WD	Two wheel drive
4WD	Four wheel drive
BP	British Petroleum
CAD	Computer Aided Design
CO_2	Carbon dioxide
CFD	Computational Fluid Dynamics
HWA	Hot-wire Anemometry
LDA	Laser Doppler Anemometry
MBC	Moving Boundary Condition
MRF	Multiple Reference Frame
RANS	Raynolds-Averaged Navier Stokes
PIV	Particle Image Velocimetry
TU	Traversing unit

Thesis

This thesis consists of an extended summary and the following appended papers:

Paper A Sterken, L., Sebben, S., and Löfdahl, L. *Alternative Approach in Ground Vehicle Wake Analysis. World Academy of Science, Engineering and Technology* 68 (2012)

Paper B Sterken, L. et al. *Experimental and Numerical Investigations of the Base Wake on an SUV. SAE World Congress* 2013-01-0464 (2013)

Contents

List of Figures

List of Tables

1 Introduction

This chapter gives the background of the project showing the relevance of the research. It also summarizes the project goals.

1.1 Background

It is not surprising to realize that the development of today's society goes hand in hand with an increasing energy consumption. Throughout the last decades the total energy consumption has seen a steady global rise. This growth is most noticeable in the new economic regions such as Asia and Non-OECD (Organisation for Economic Co-operation and Development) Americas; whereas in the OECD countries consumption has stagnated [1, 2].

Different fuel sources are utilized to meet the global needs in energy, but oil takes a significant one-third share of the total energy consumption [3]. If the contribution from oil is further divided into sectors, it becomes clear that the transportation sector plays a significant role in the total oil usage and is increasing its share[2].

The combined effect of oil as the main energy source, and the transportation sector as the main consumer within it indicates that it is a key area for improvement when looking for ways for reducing the environmental footprint. For instance, in Europe passenger cars are responsible for approximately 12% of the total EU emissions of CO_2 [4]. Therefore over recent years legislation has been put in place to reduce the environmental impact of transportation. The achieved fleet average of new cars is required to be 130 g/km of CO_2 by 2015 and 95 g/km by 2020. Penalties have been introduced for each registered car that does not meet these targets. This regulation is also planned for implementation into a more general 20-20-20 legislation that states that the CO_2-production and fuel consumption of vehicles should be 20% less by the year 2020 [4, 5].

Another negative impact on transportation's dependency on oil is the increase in oil prices in recent years. Figure 1.1 shows the evolution of the price over the last 150 years. Two peaks can be seen in the oil prices. The first one took place at the end of 1970's as a consequence of the Yom Kippur war and the Iranian revolution. The second peak coincided with the invasion of Iraq in 2003 and is still present with high oil prices at the time of writing [6].

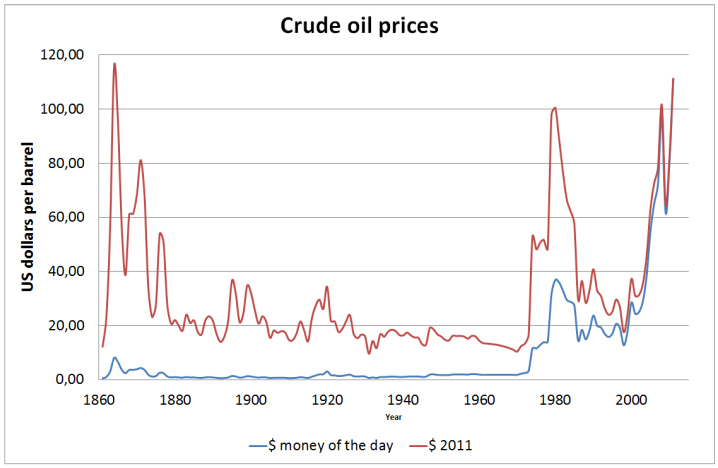

Figure 1.1: *Oil price per barrel in $US [6]*

Both situations of increasing fuel prices and tougher legislation cause vehicle manufacturers to continue to reduce fuel consumption and hence CO_2-emissions. One direction for improvement is to look at the propulsion system of the vehicle. Research is being conducted into alternative fuels, more-efficient combustion engines and new propulsion techniques. These studies have resulted in vehicles running on alternative more eco-friendly fuels, hybrid vehicles or even pure electric vehicles. A second option for reduced fuel consumption is to decrease the driving resistance. A more detailed explanation of the driving resistance follows in Chapter 2, but one component contributing to the overall resistance is the aerodynamic drag. How efficient a car is aerodynamically, can be expressed by its non-dimensional value C_D or drag coefficient. Figure 1.2 gives an historical overview of the evolution of the drag coefficient over the last decades, showing a downward trend. Of note is the drop in C_D at the end of the 1970's, early 1980's that followed a period of increased fuel prices, see Figure 1.1. In recent years the drag coefficient has only experienced a slow decrease. With the use of conventional methods based on vehicle design the drag coefficient has experienced an asymptotic trend towards a C_D~0.2. The increase in fuel prices, but even more so, the CO_2 legislation with possible penalties has stimulated vehicle manufacturers to find innovative methods to further decrease C_D. These methods include (actively) controlling the flow around the vehicle in order to reduce the air resistance and/or increase stability at higher speeds.

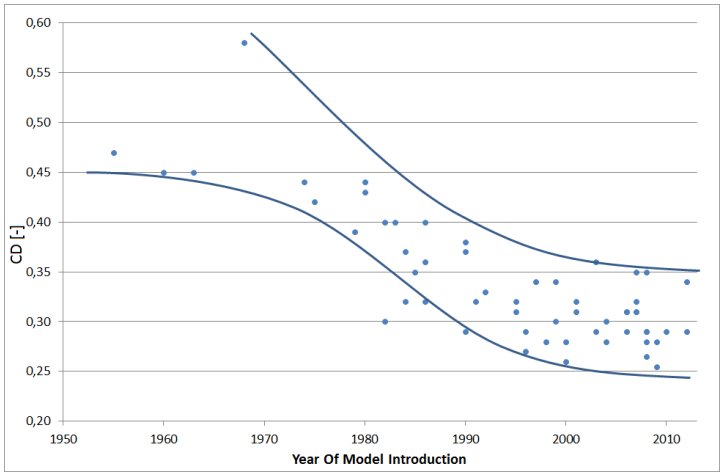

Figure 1.2: *Vehicle C_D-history over last 50 years (Courtesy of Volvo Car Corporation)*

1.2 Project motivation

Stated in the previous section, vehicle manufacturers must find new methods to further reduce emissions and hence fuel consumption. Besides lighter materials or a more efficient powertrain, aerodynamics can contribute achieving the goals, set by legislation. Since vehicles can be treated as a bluff body, the flow will experience separation at the rear end. This creates a large wake region behind the vehicle body. As a consequence most of the aerodynamic resistance is caused by pressure drag [8, 9]. In fact, as much as 85% of the drag can be attributed to pressure drag [9].

Logically, the wake behind the vehicle is influenced by the flow around the car. Perhaps it can be said that the flow around the exterior is well understood, but this is definitely not the case for underbody flow, wheel flow or engine bay flow with the presence of a cooling package. Lately quite a lot of research has gone into the understanding of their effects onto the local flow field and their contribution to the global drag. Some papers investigating the effects of wheel aerodynamics are given in [10, 11, 12] , underbody flow [13, 14] or engine bay flow [15, 16, 17].

In recent years, the importance of a moving ground with rotating wheels has been demonstrated for correctly representing the flow around the car. Therefore wind tunnels are being equipped with moving ground systems. Wheel rotation and a different boundary condition in the underbody naturally also has an effect on the base wake.

Nevertheless, the rear vehicle wake has never been ignored and focus has increased in order to gain insight in the time-dependent wake structures of different vehicle types, or to find methods of reducing the aerodynamic drag by changing the base area of the vehicle.
Therefore, it is clear that the wake behind the vehicle contains crucial information

how the flow transports its energy around the car, and where the highest energy losses take place.

1.3 Project goals

The main goal in this research project is to gain an understanding of how the wake of a vehicle can be controlled and optimised, resulting in a drag reduction. To accomplish this, an understanding of how the wake structures propagate in time and in space is required together with the parameters that influence these structures. Therefore wind tunnel and Computational Fluid Dynamics (CFD) methods will have to be improved or, where necessary, new methods will have to be developed to capture these unsteady wake effects. A correlation between the two methods can be made after which they can be used side-by-side for the development of new concepts.

Innovative concepts and/or devices will be implemented near the base area of the car to control the flow entering the base wake, such that drag is reduced or high-speed stability is obtained. The effect of these devices on the flow will be investigated both in the wind tunnel and in numerical simulations.

Furthermore the aim is to isolate and understand the individual contributions of the different wake zones (exterior, underbody, wheels) and their interactions. The parameters or areas in the rear wake with the largest effect on the drag coefficient will be identified.

2 Aerodynamics of passenger cars

This chapter will first give a literature overview related to base wake investigations. In the second section the importance of the wake in relationship to the aerodynamic drag will be given as part of the driving resistance of a vehicle.

2.1 Literature review

The intention of this section is to give an overview of those papers that have influenced this research in the direction it has taken. These papers involve not only investigations that have been conducted in a wind tunnel, but also studies with the use of Computational Fluid Dynamics. This section will start with an explanation of the experimental papers; the numerical papers can be found in the second part.

One of the first investigations on wake shapes and the complex structures emanating close to the car's rear end was conducted by Ahmed and others [19, 20]. These extending studies were applied to three vehicle types: a notchback, fastback and squareback. With a 2 mm thick plate placed in the wake of the models at symmetry, a qualitative impression of the wake structures in the symmetry plane could be made. To retrieve quantitative flow information a 9-hole pressure probe was inserted in the base wake to measure the pressures in several transverse planes at different distances behind the models. Here, the in-plane velocity vectors together with the position of the vortex cores could be determined and the contribution of the vortex drag could be calculated.

With the aid of a 14-hole pressure probe, a more quantitative analysis of the wake structures could be made in the Pininfarina wind-tunnel. This technique enabled the researchers to measure the local velocity angle and pressures at low velocities and even reversed flow, with less sensitivity to the oncoming flow. A detailed description of the pressure probes can be found in [18]. Simultaneous with their development of the probes, post-processing improvements were made by introducing a new visualization variable, Microdrag, based on the momentum equation [21].

Using the local drag information found in a transverse plane, a new technique, called the fluid tail technique (FTT), has been developed looking for a more balanced wake in order to reduce the drag of a car [22]. Parameters for obtaining a more balanced wake are:

- Base perimeter should be circular or elliptical.
- Separation should occur as close to base perimeter as possible.
- Separation should be transversal to the vehicle's direction of motion.
- Similar flow conditions in pressure and velocity should occur over the perimeter.

The time-dependent nature of the wake structures were coupled to the dominant flow frequencies in several unsteady investigations [23, 24, 25, 26, 27, 28].
More specifically for a squareback investigation model [23], the characteristic vortex shedding frequency was measured to be approximately $St = 1.157$, and the frequency of closure region pumping effect around $St = 0.069$. The phenomenon of vortex pairing occurs where vortices merge while travelling downstream. This pairing reduces the characteristic frequency by a half and increase their size.
Unsteady wake measurements on a more SUV-shaped model have been conducted in [29, 30].
It also has been found that the surface pressure fluctuations on the models were smaller than the wake pressure fluctuations, making the surface fluctuations harder to be detected [24, 28].

Other investigations looked at methods applied near the base area of the bluff body to reduce the aerodynamic drag. Most common approaches were boat-tailing, base bleed, cavities, or splitter plates [31, 32]. The studies, that were carried out at small-scale, gave promising results with these approaches, but when the same technique was applied on a full size passenger vehicle no significant reduction in drag could be observed.
For instance, when base bleed was applied on an SUV in a full-scale wind-tunnel, no significant drag reduction could be achieved [33]. In the same paper the application of cavities was shown to be more effective to reduce drag, but the increased friction drag cancelled out most of the gain from the increased base pressure.
Another example was the attachment of small strips to the base in order to limit the near-wall flow. Applied on a small scale model a drag reduction could be observed, but on a full size squareback vehicle the same effect was not noticed [34].
Hucho [8] gave other examples that did not improve drag on real cars, as would have been expected from small scale. This shows the increased complexity of full-size models with rotating tyres and moving ground, and the difficulty in finding innovative methods for drag reduction on passenger vehicles.
One theory for the mis-match between full size and scale could be explained by the underbody roughness [35, 36]. This gained renewed attention by Perry [37].

To close the gap between scale-model results and full-size results, a new reference model has been developed by merging the geometrical characteristics of two passenger vehicles. The resulting model, called the DrivAer model, can be configured as a notchback, fastback and squareback. The representation of the flow around the model is more realistic than the one obtained by using more simple automotive reference models described in [38]. The model allows the investigation of the unsteady flow structures around and behind the car, as well as helpiing the search in innovative modifications to the vehicle to accomplish drag reduction [39, 40, 41].

The effects of the cooling-package on the global drag and base wake have been studied as well. The exit location, and the design of the engine-bay outlet to the underbody, influence the global drag and the total pressure distribution in the wake behind the vehicle. These effects could both be seen in a transverse plane behind the vehicle or in a symmetry plane located in the wake. Comparisons with a closed-cooling configuration, reveal that the location of the vortices associated with a toric structure close to the base surface moves more downstream with a lower cooling drag contribution to the total drag [15, 16, 17].

2.2 Driving resistance

The driving resistance is determined by equation 2.1.

$$F_D = m\frac{dV}{dt} + f_r mg\cos(\alpha) + mg\sin(\alpha) + C_D\frac{1}{2}\rho V_\infty^2 A = F_A + F_R + F_G + F_D \quad (2.1)$$

The first term in Equation 2.1 is the inertial force and is called acceleration resistance. A passenger vehicle undergoing a driving cycle experiences a substantial effect on its driving resistance due to this term. The second term is referred to as the rolling resistance and is linearly dependent on the normal contribution of the gravitational force to the road surface. The f_r-parameter in this term is the rolling resistance coefficients. Though this parameter is often treated as a constant, in reality it is very complex and dependent on several factors such as speed, load, tyre pressure and road surface. The parallel contribution of the gravitational force to the road surface represents the climbing resistance of the vehicle. The fourth term is the aerodynamic resistance. The density and frontal area show a linear contribution to the aerodynamic resistance, whereas velocity has a quadratic effect. To close the equation, these contributions are multiplied by a drag coefficient C_D. This coefficient can be used to compare the aerodynamic efficiency of two vehicles, but for fuel consumption it can be more useful to compare the product $C_D S$.

From Equation 2.1 it is obvious that weight is a crucial parameter for the driving resistance. It plays a role in the first 3 out of 4 terms. Hence, a weight reduction would mean a significant reduction in the driving resistance.
However, in steady driving conditions on a level road the total driving force simplifies into a rolling- and aerodynamic force, which are the second and fourth term in Equation 2.1. Figure 2.1 shows the behaviour of both these forces relative to speed. At around 65-70 km/h the aerodynamic force becomes the most dominant term.

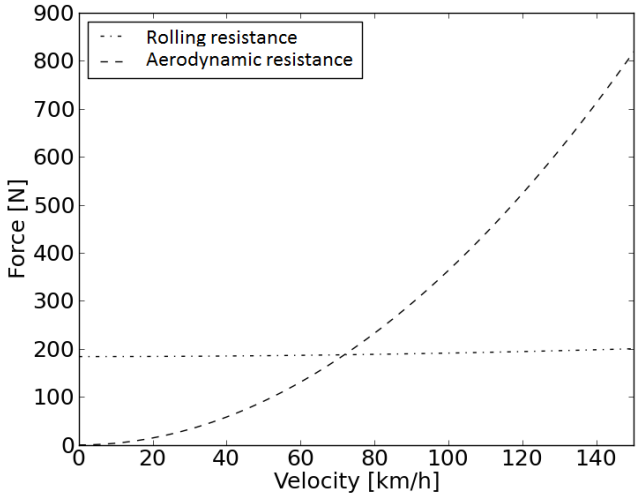

Figure 2.1: *Driving force example, assuming steady velocity on level road*

The aerodynamic drag acting on the surface of the vehicle can be divided in two parts. A friction force is caused by the interaction between the fluid (air) and the surface of the vehicle. This creates a boundary layer where kinetic energy is converted into heat. This shearing force acts parallel to surface with its longitudinal component contributing to the drag. Another force, acting normal to the surface, is created by the pressure on that surface. The force resulting from the pressure difference working in the longitudinal direction is called pressure drag. Due to the shape of the vehicles being characterised as bluff bodies, pressure drag is the main contributor to the overall drag. The importance of the wake in the pressure drag can be shown by a C_D versus x plot of the drag force on the surface of the car, given in Figure 2.2. A sharp increase in drag can be seen at the rear of the vehicle ($X > 4$), starting around the rear axle. The increase can be explained by the negative pressure on the base area due to the separation of the air and the creation of a wake.
Also visible in Figure 2.2 is the contribution of the exterior to the overall drag. Around 45% of the drag is produced by the exterior. This means that more than half is produced by other regions, such as under body and wheels.

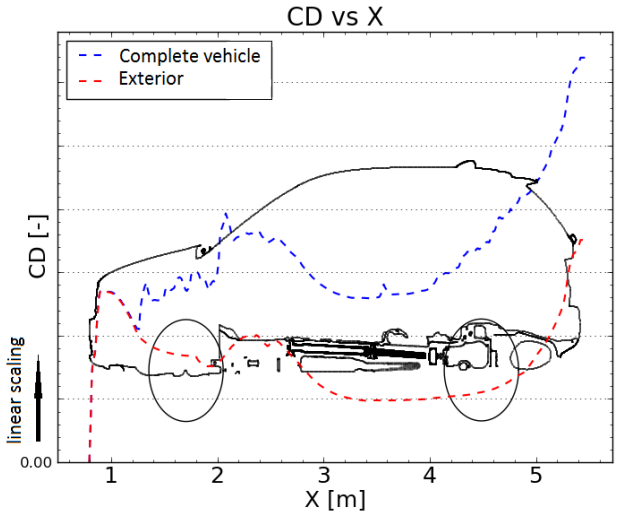

Figure 2.2: *Example of a C_D vs X*

3 Methodology

This chapter will provide a closer look at the methods used in this research. It will be split in an experimental set-up overview and a numerical procedure explanation.

3.1 Experimental setup

First a more detailed explanation of the wind tunnel layout will be given. Afterwards, an overview is given of the equipment used in the experiments.

3.1.1 The Volvo Cars Aerodynamic Wind Tunnel

All experiments were conducted in the Volvo Cars Aerodynamics Wind Tunnel. This tunnel is a full-scale wind tunnel with a slotted wall configuration. It is equipped with a moving ground system, together with an improved installation of boundary layer suction and tangential blowing equipment. The moving-ground system has been designed by MTS and consists of 5 belts: one belt for each wheel, and a centre belt under the vehicle. This improves on the production of the correct flow under the car and in the wake of the car, as a number of researches have shown [10]. At the start of the test section a scoop has been placed to remove the initial boundary layer created in the settling chamber and contraction. In the test section, the ground has holes to keep the boundary-layer growth to a minimum. Behind each of the belts a tangential-blowing device is installed to re-energize the boundary layer. A more detailed description can be found in an SAE paper published in 2007. A sketch of the wind tunnel can be seen in Figure 3.1a, with a representation of the installed moving ground system in Figure 3.1b.

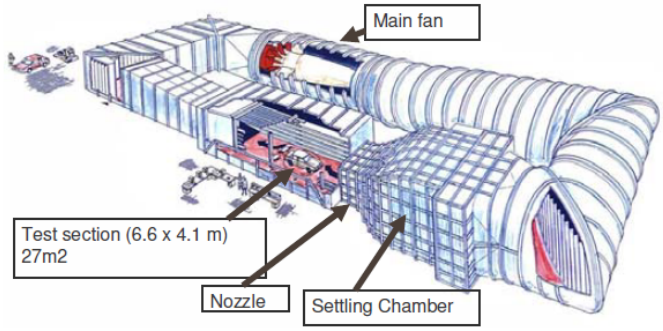

(a)

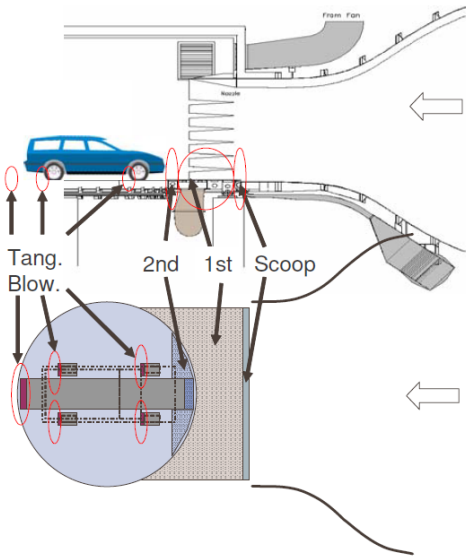

(b)

Figure 3.1: *Volvo Cars Aerodynamic Wind Tunnel: (a) Wind Tunnel sketch, (b) Ground simulation system sketch. [43]*

3.1.2 Test objects

During the first year of the research it was decided that the Volvo XC60 would be used in the investigations. In a very early design-phase of this vehicle, while still investigating prototypes, it was observed that some configurations experienced detrimental unsteady effects, causing stability issues at high speeds and increased air resistance. Whereas these effects were absent on the final production version, it was considered a good choice since the car could be altered back to these early configurations in order to investigate the undesirable unsteady effects. A numerical model representation can be seen in Figure 3.2.

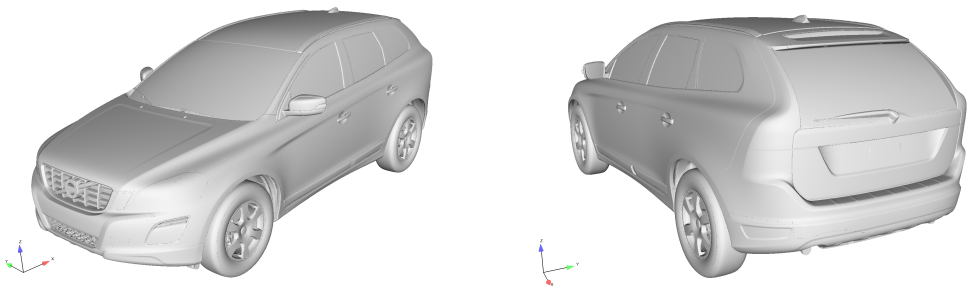

(a) (b)

Figure 3.2: *Volvo XC60 model representation: (a) Front iso view, (b) Rear iso view.*

Also, a difference in drag has been noted between the the 2WD and 4WD versions when measured in the wind tunnel, which gave an extra parameter to investigate. The main geometric differences between the two versions can be found in the engine undershield, the engine downpipe, fuel tank, exhaust system and the additional rear differential and driveshafts. An underbody view of the 2WD and 4WD versions can be seen in Figure 3.3.

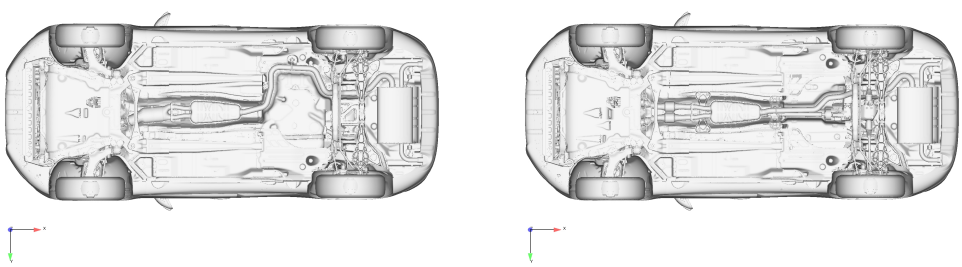

(a) (b)

Figure 3.3: *Volvo XC60 underbody differences: (a) 2WD, (b) 4WD.*

3.1.3 Investigated configurations

Four configurations were chosen to be investigated in this research. These cases being the open-cooling, closed-cooling, closed-front, and an extended roof spoiler. With open-cooling as the base configuration, as seen in Figure 3.2, this meant no additional modifications.
To create the closed-cooling arrangement, the upper and lower grille were covered with a metal plate and sealed with tape. The modifation can be seen in Figure 3.4a.
In addition to the closed-cooling changes, to obtain the closed-front case all flow interaction with the engine-bay was blocked. The engine-bay flow to the underbody was obstructed by inserting foam above the front axle, visible in Figure 3.4b, while the flow interaction with the front wheelhouses was stopped by installing plastic covers. An example of these covers can be seen in Figure 3.4c. In order to close the engine-bay completely the NACA ducts and cooling hole in the engine undershield were taped over. The closed-front configuration is a combination of Figure 3.4a, Figure 3.4b and Figure 3.4c.
The fourth configuration was a modified open-cooling configuration through the addition of a roof panel, covering both the roof step (with the third brake-light) and the integrated duck-tail spoiler. The cover had an extra 0.2 m extension behind the integrated roof spoiler. Figure 3.4d shows the extended roof spoiler.

The closed-cooling case removed the contribution of the cooling package to the total drag. It altered the mass flow distribution around the car which caused an effect on the wake behind the vehicle.
The additional step of making the vehicle closed-front in the wind tunnel was to compare the results with the numerical simulations. In CFD it is a more common approach since it reduces the resource requirements by not having an engine-bay mesh. Also in the case of the Volvo XC60, a significant drag reduction in CFD was observed compared to the closed-cooling. So an attempt was made to reproduce the closed-front configuration in the wind tunnel.
The extended roof spoiler was attached to the roof of the car in order to remove the detrimental effects of the roof step and integrated duck-tail spoiler on air resistance. The 0.2 m extension helped to improve the pressure recovery over the roof of the vehicle and delayed the separation point. The extension was shaped to follow the roof curvature. In CFD, extra simulations were conducted with a combination of extended roof spoiler and diffuser, but no real improvements could be seen. Therefore it was decided to keep the configuration with only the roof spoiler.

In the wind tunnel, the first three configurations in both the 2WD and 4WD variant were used to take surface pressure measurements. They were subjected to a Reynold sweep, yaw sweep, and configurations with stationary/rotating wheels. This created a database with base pressure measurements and corresponding force values that could be used for correlation with the numerical simulations in the development of an unsteady CFD approach for aerodynamics.
The open- and closed-cooling, together with the extended roof spoiler configuration in the 4WD variant were used to conduct the wake measurements.

(a)

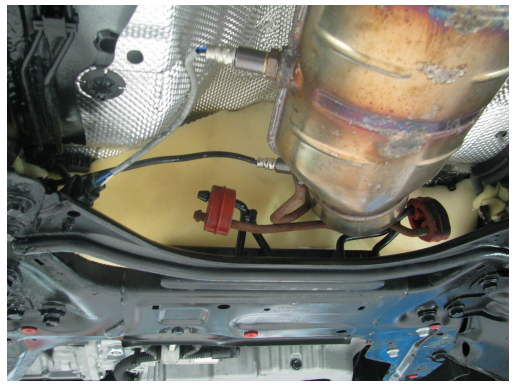

(b)

(c)

(d)

Figure 3.4: *Volvo XC60 configuration changes: (a) Closed-cooling, (b) Closed engine bay to underbody, (c) Closed engine bay to wheelhouse, (d) Extended roof spoiler*

3.1.4 Measurement equipment

Several techniques can be applied to improve the understanding of the flow around the car. These techniques can produce qualitative or quantitative information, being time-dependent or time-averaged results. Depending on the chosen technique, the measurement equipment can be intrusive or non-intrusive to the flow.

At the start of this research several techniques were considered. As a requirement to meet the scope of this investigation, they had be able to give quantitative unsteady information. Therefore Hot Wire Anenometry (HWA), Laser Doppler Anenometry (LDA), Particle Image Velocimetry (PIV) and pressure measurements were considered. The HWA approach can give valuable results in unsteady measurements, but the probes are sensitive and difficult to calibrate. The LDA technique is non-intrusive but the equipment is expensive and was not available at Volvo Car Corporation. The PIV approach can produce flow results of a specific frame area quickly, but has the disadvantage that these frame areas are relatively small compared to full-scale vehicle. Consequently many frames have to be taken in order to capture the overall wake flow. Plus, the number of particles required to capture the flow satisfactory in a thin laser sheet can be large. The technique based on pressure measurements on the other hand can be used to retrieve time-averaged or unsteady quantitative results, both on the surface of the car and in the flow around the car.

Therefore all flow-field measurements were conducted using the pressure system currently available at the Volvo Cars wind tunnel. The system is a PSI 8400 pressure scanner system from Pressure Systems Inc, with specification details that can be found in [46]. The system works together with PSI ESP Pressure Scanners, see details [47]. For the surface measurements, the system was set up with a 10 Hz sampling rate for a duration of 20 s. This is equal to the balance force measurements. The wake measurements were configured with a 10 Hz sampling rate for 3 s. This duration was a balance between measurement time per wake point and available wind tunnel session time for all planes of all configurations.

On the surface of the car a combination of drilled holes and pressure spades were applied to investigate the base pressures under different circumstances. Since drilled holes take more time to prepare, only those regions on the car that really benefit from them were prepared in that way. These being the regions before separation, such as roof, rear lamps and bumper, resulting in as little effect on the oncoming flow as possible. The trunk of the car consists of pressure spades since it is immersed in the vehicle wake. The pressure locations were chosen with a focus near the separation regions, since most flow information influencing the wake flow can be retrieved from these positions.
The individual parts could be exchanged between the two vehicles to speed up the installation process while changing from one vehicle to the other. A representation of the surface pressure locations can be seen in Figure 3.5a, with a close-up of the rear lamp in Figure 3.5b.

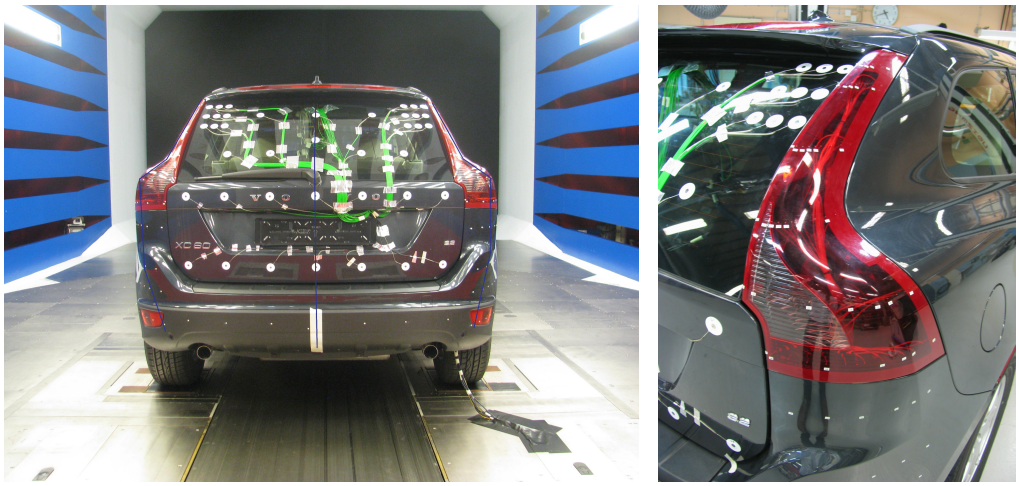

(a) (b)

Figure 3.5: *Pressure point locations base: (a) Overview of base pressure points, (b)Pressure points around rear lamp.*

To measure the wake flow in the wind tunnel, two 12-hole pressure probes, or omniprobes, were attached to the traversing unit of the wind tunnel. These probes were capable of measuring the flow up to ±160° cone angle with a flow angle accuracy better than 0.1% and total flow velocity accuracy of better than 1.0% [44, 45]. The probes were placed at an angle of 45° so that fully reversed flow could be measured. An example of the omniprobes mounted on the traversing unit in the wind tunnel can be seen in Figure 3.6.

Figure 3.6: *Traversing unit with omniprobes*

In order to investigate the wake shape and wake size, three planes were chosen to visualise the wake: a transverse plane 0.1 m behind the vehicle, a symmetry plane, and a horizontal plane at 0.824 m (near top of wheelarch). Even though a fourth (horizontal) plane was obtained due to the vertical orientation of the two omniprobes, only the upper plane was studied since no obvious differences in flow field between the two could be observed. The point distribution in each plane was chosen such that it was concentrated where the expected shear layer and/or closure region were located. To identify the closure region location, a line sweep progressing with discrete steps backwards away from the car's rear end was conducted at the start of the first configuration. The three planes are referred to henceforth as Xplane, Yplane and Zplane respectively. The wake planes are shown in Figure 3.7, and their dimensions are given in Table 3.1.

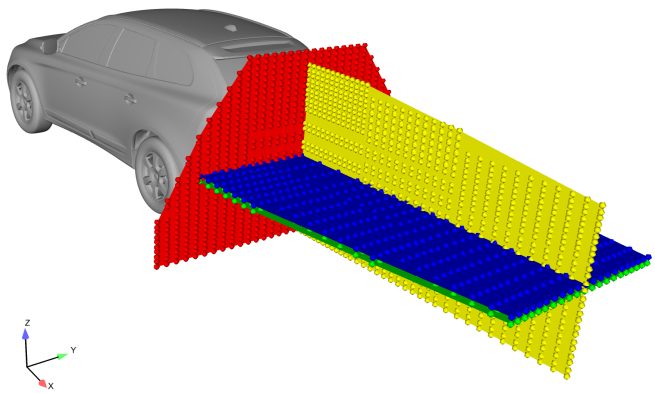

Figure 3.7: *Investigated wake planes*

Table 3.1: Wake dimensions

Wake plane	**Dimensions**
Xplane	Width: 3 m by Height: 1.8 m
Yplane	Length: 3 m by Height: 1.65 m
Zplane	Length: 3 m by Width: 2.2 m

3.2 Numerical procedure

In the initial phase of the investigations the standard Volvo Cars procedure was used. This procedure is explained in the first section. Following, a quantification approach for wake analysis is explained.

3.2.1 Standard procedure

The Computer Aided Design (CAD) models of the parts of the physical vehicles from the experiments were downloaded from the Teamcenter database. These parts were merged together in ANSA, where they were cleaned, surface meshed and prepared for volume meshing. The tyres were CAD representations of the mould the tyre were made in, received courtesy of the tyre manufacturer. These tyres were morphed in ANSA following the morphing procedure as described by Sebben [48]. The morphing were based on picture comparison of tyre deformation changes between a stationary- and rotating wheel during the wind-tunnel tests. By counting pixel differences between the two pictures the tyre deformation could be calculated. After the completion of the ANSA preparation, a volume mesh was then created in HARPOON. The end result being a mesh consisting of between 50 million to 90 million cells, depending on the configuration. Each case was solved in ANSYS Fluent using the realizable k-ϵ turbulence model with standard wall functions, following the guidelines first described by Chronéer [49]. Wheel rotation was treated according to the guidelines of Sebben [48]. The tyre and outer wheel rim were given a rotational Moving Boundary Condition (MBC), whereas the inner rim between the spokes remained stationary. In this latter region it was the fluid that was given a rotational velocity by introducing a Multiple Reference Frame approach (MRF) in the zone between the spokes. Post processing of the results was conducted in ENSIGHT, Python and Excel.

3.3 Post processing parameters

3.3.1 Local drag

Newton's third law states that every action has a reaction. This implies that for the force the flow is exerted on the car, the car applied an equal force on the flow. As a consequence, the vehicle's drag coefficient can also be calculated by using the information found in the flow. Starting from Newton's second law, the local drag in the flow can be written according to equation 3.1. A derivation of this formula can be found in a paper published at the VKI in 2005 [50].

$$C_{D_{wake}}A = \int_S \underbrace{(1 - c_{p_{tot}})}_{I} dS - \int_S \underbrace{\left(1 - \frac{V_x}{V_\infty}\right)^2}_{II} dS + \int_S \underbrace{\left(\frac{V_y^2 + V_z^2}{V_\infty^2}\right)}_{III} dS \quad (3.1)$$

The first term in equation 3.1 is the local energy losses in the flow from the total pressure; the second term is the local longitudinal velocity energy losses; and the third term can be considered the cross-flow drag. The first two terms together can be seen as form drag or pressure drag. Therefore air resistance can be reduced by decreasing the wake size, local total pressure losses or by limiting the rotational kinetic energy losses [50].

3.3.2 Integrated local drag on polar mesh

Similar to a C_D versus X plot, the idea with the polar plot is to look at the drag contribution of the different wake regions and retrieve a C_D^* versus θ plot. How the shear layer is positioned with respect to a chosen origin makes it easier to differentiate between the regional drag contributions. It also allows for quantification of the wake based on the ratio of the integrated local drag of each θ section to the total integrated local drag for all θ, expressed in percentage, as can be seen in Equation 3.2.

$$C_D^*\text{-ratio} = \frac{\int C_D^* d\theta}{\int_0^{360} C_D^* d\theta} * 100 \quad (3.2)$$

The Xplane 0.1 m behind the vehicle is transformed into polar coordinates results based on the approach as described in Paper A [51]. Initially, the method was developed on vehicles with no wheels and filled wheelhouses. But gradually it has been applied to more complex models until finally it has been applied to a fully-detailed one. Figure 3.8 shows the progression from a cartesian coordinate plane to a C_D^* vs θ plot for a sedan-type vehicle. The polar plot in Figure 3.8b shows the same wake structure from the different geometrical regions as Figure 3.8a. In polar coordinates these regions can be divided between fixed θ-ranges, which are only car-type dependent. For the sedan vehicle in this example, the regions can be split by roof (90° to 135°), side mirror (135° to 160°), side (160° to 200°), wheel (200° to 250°) and underbody (250° to 270°). This regional division allows for a local drag integration as a function of θ on the polar mesh, seen in Figure 3.8c.

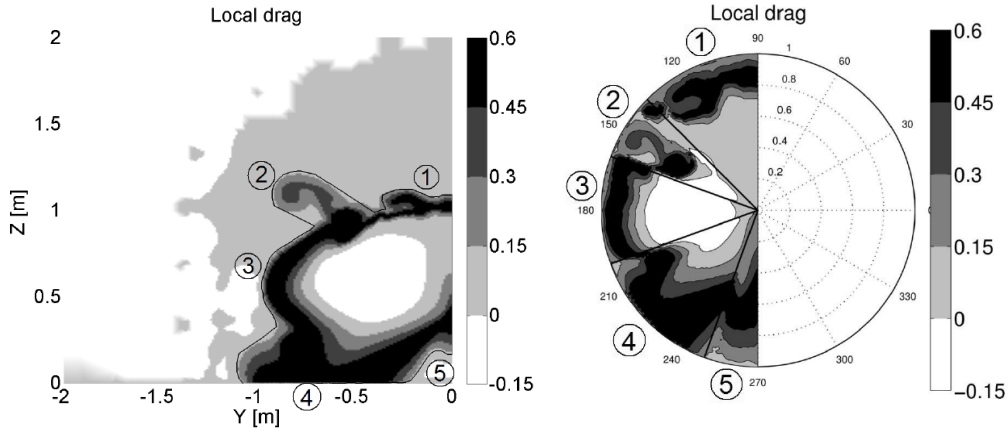

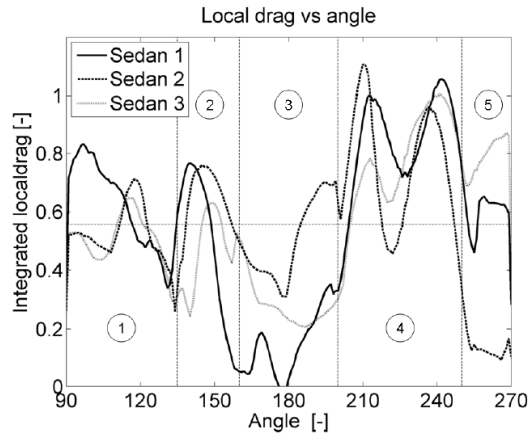

Figure 3.8: *Steps from cartesian plot to C_D^* as a function of θ: (a) Cartesian Xplane, (b) Polar Xplane, (c) C_D^* vs θ. [51]*

After a gradual increase of the number of C_D^* versus θ plots on a range of simplified to detailed configurations, gave an increased familiarity with the plots, the method was applied on the other simulations with the XC60.

4 Results

This chapter describes the experimental and numerical results, as conducted on both versions of the XC60. In the first part the experimental results are given. In the second, the results of the numerical simulations are discussed.

4.1 Experimental results

In this section the most relevant wind tunnel results will be discussed. First a global drag comparison is given. After, the base-surface and base-wake measurements are discussed respectively. While conducting the wake measurements, interference effects of the traversing unit on the balance forces were noted. These are discussed in the third section.

4.1.1 Global drag

Throughout the thesis four main configurations, as described in Chapter 3, were investigated. These configurations show a significant difference in C_D-value, given in Table 4.1 for both vehicles. For comparison between the configurations, the C_D-values are given for both vehicles separately. However, in order to compare both vehicles, it is sufficient to know that the 4WD open-cooling showed a 6 drag count reduction ($\Delta C_D = -0.006$) with the 2WD open-cooling variant.
As expected removing the cooling-air flow decreases the air resistance significantly as there is no air moving through the cooling package. Making the vehicles closed-front had little effect on the drag value compared to the closed-cooling in the experiments.

Table 4.1: Drag coefficients for experimental configurations

Configuration	ΔC_D 2WD	ΔC_D 4WD
Open-cooling	reference	reference
Closed-cooling	-0.015	-0.013
Closed-front	-0.014	-0.017
Extended roof spoiler		-0.005

4.1.2 Surface measurements

As described in Chapter 3, surface pressures were taken at the base and symmetry line of both the 2WD and 4WD. Figure 4.1 shows the base pressure for the open cooling- and closed cooling configurations. The base pressure decreased in the closed-cooling configuration compared to the open-cooling. This was due to the increased mass flow around the car. Even though not shown, the closed-front case showed the same behaviour as the closed-cooling.

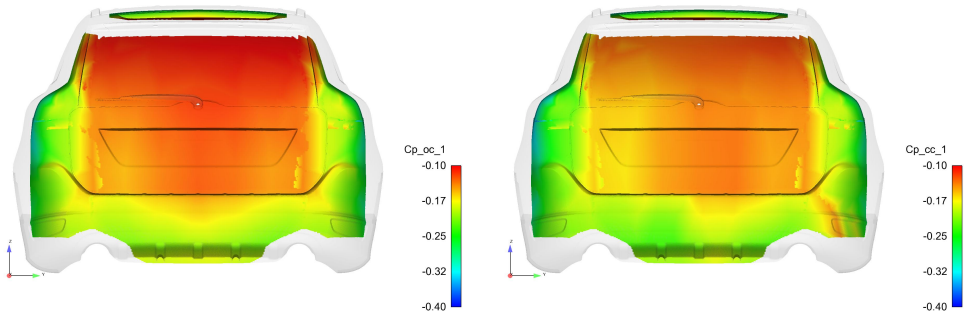

(a) (b)

Figure 4.1: *C_p on base 4WD from experiments: (a) Open-cooling, (b) Closed-cooling.*

Figure 4.2 shows the standard deviation of the base pressure for the same cases. Here the closed-cooling revealed a higher fluctuation of the pressures. The flow still contained more energy when it reached the base of the vehicle in the closed-cooling configuration. This higher energy flow from different regions around the car interacted with each other, resulting in larger variations of the pressure.

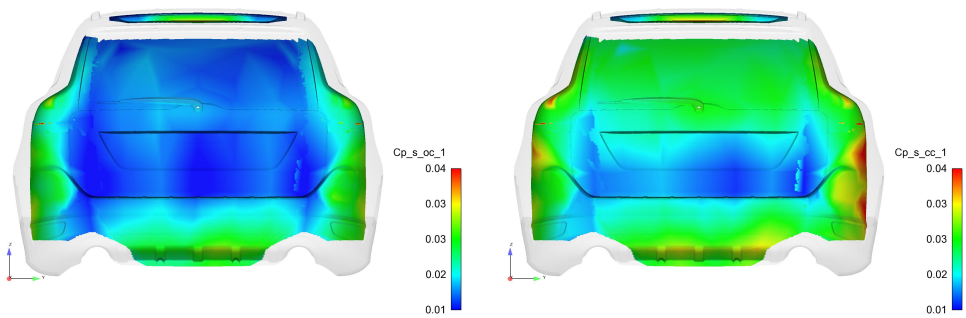

(a) (b)

Figure 4.2: *C_{p_s} on base 4WD from experiments: (a) Open-cooling, (b) Closed-cooling.*

4.1.3 Wake measurements

For the multiple planes as discussed in Chapter 3, the outcome for the experimental results is discussed in next subsection. The effect of the traversing unit's presence on the balance forces is given in the second subsection.

Experimental wake planes

Figure 4.3 shows the transverse wake plane 0.1 m behind the vehicle for the open- and closed-cooling. The effect of the cooling drag can be seen in the flow resulting from the underbody. The open-cooling configuration had two separate low drag regions, while these merged into one single region in the closed-cooling. An additional effect was the reduced wake width of the wheel wakes.

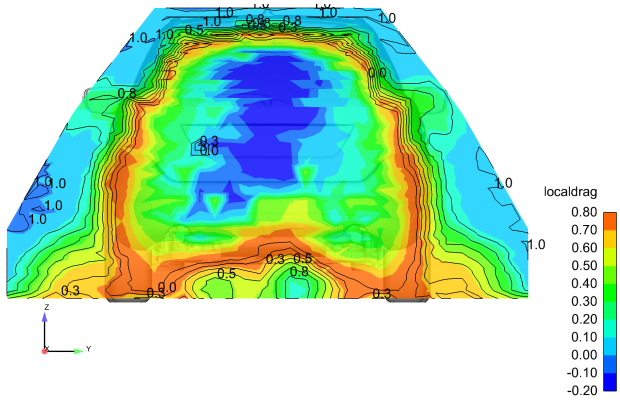

(a)

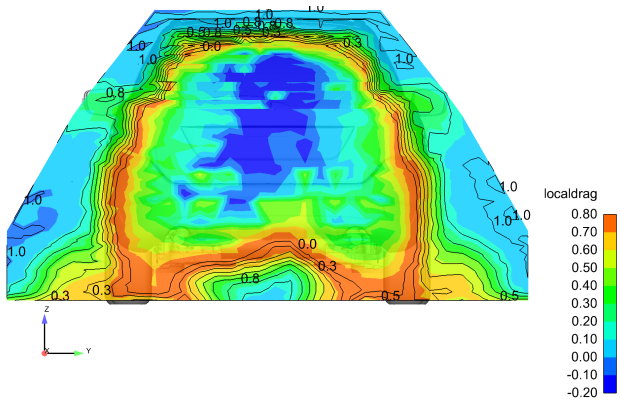

(b)

Figure 4.3: *Local drag superimposed with $c_{p_{tot}}$-contour lines for an Xplane in WT: (a) Open-cooling, (b) Closed-cooling. [52]*

The roof-spoiler configuration compared to open-cooling for the Yplane is given in Figure 4.4. The 0.2 m extension increased the inclination of the roof flow more in a downward direction and improved its pressure recovery. The delayed separation caused the shear layer to remain thinner in the near wake. In the far wake it reduced the wake height. It can also be seen that the chosen height of 1.8 m was not high enough close to vehicle for the open-cooling case. The shear layer was not fully captured, and the freestream energy is not reached at the top of the plane.
Identified in the Yplane by a black dot is the wake closure region. For all three configurations, the wake closure region was located approximately 1.6 to 1.7 m behind the vehicle.

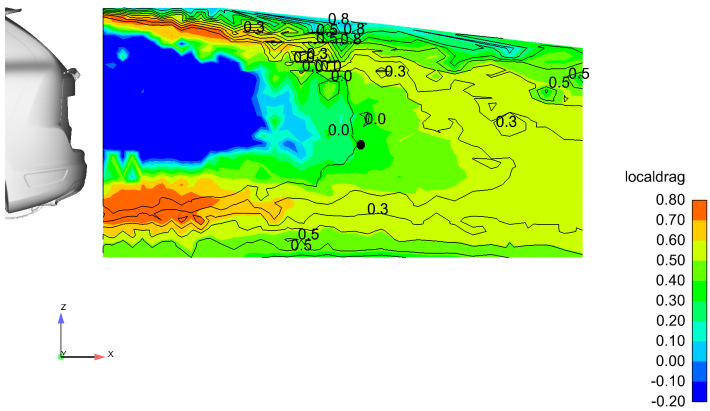

(a)

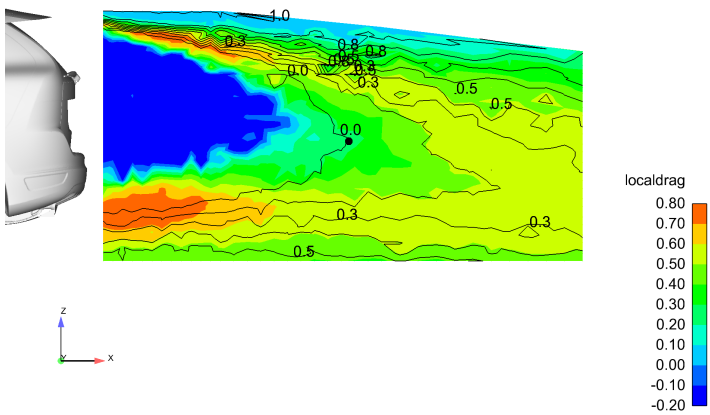

(b)

Figure 4.4: *Local drag superimposed with $c_{p_{tot}}$-contour lines for Yplane in WT: (a) Open-cooling, (b) Extended roof spoiler. [52]*

Effect on balance forces

The drag force measured by the balance system and as a function of the traversing unit's position, for the Xplane and Zplane, is shown in Figure 4.5. The ΔC_D is defined as the drag coefficient measured by the balance system with the traversing unit in place compared to the reference configuration with the traversing unit in its parking position, so $\Delta C_D = C_D - C_{D_{ref}}$. Figure 4.5a shows the effect in the Xplane. While measuring points on the right side, the traversing unit was positioned outside the vehicle's wake. This increased the blockage inside the wind tunnel. Another effect was the presence of streak lines, which followed the direction the traversing unit moved. In the horizontal plane, Figure 4.5b, these streak lines are even more clearly visible. The flow seemed to change *modes* depending whether the probes were close to the vehicle or more far away. The balance also measured a lower drag coefficient when the traversing unit was further downstream.

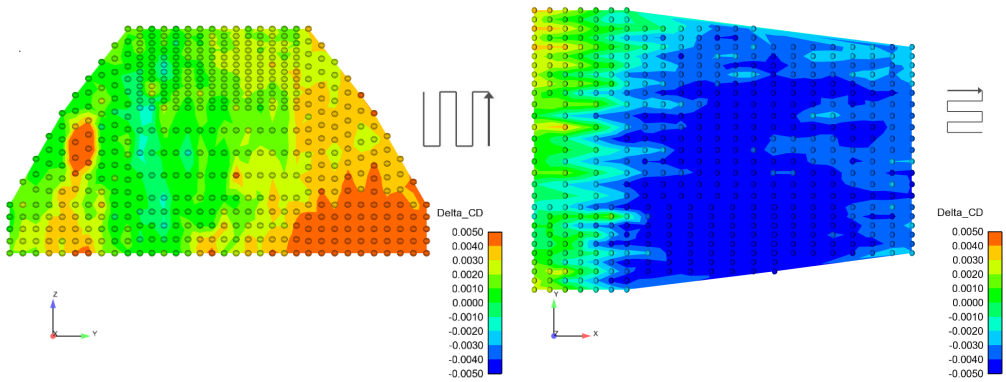

(a) (b)

Figure 4.5: $\Delta C_D = C_D - C_{D_{ref}}$ *measured by force balance as a function of probe position: (a) Xplane, (b) Zplane. [52]*

4.2 Numerical results

This CFD section follows a similar division as the experimental section based on global drag, surface-pressure measurements, and wake measurements. It compares the numerical results with the experimental results and shows in an additional subsection the result of the wake analysis method.

4.2.1 Global drag

A comparison of the drag coefficient with the coefficient obtained in the wind tunnel is given in Figure 4.6. In general, the numerical simulations predicted the drag difference between the configurations well; except for the closed-front case. Here, both the 2WD and 4WD simulations gave a significantly lower C_D-value.

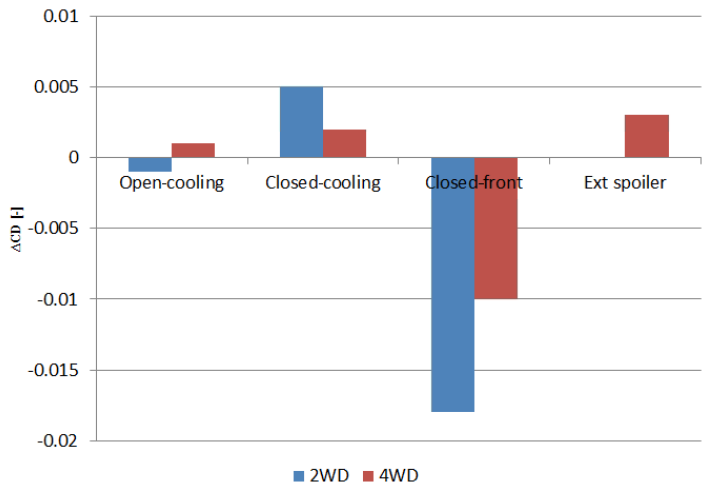

Figure 4.6: ΔC_D *CFD-WT for 2WD and 4WD*

4.2.2 Surface measurements

As with the surface-pressure measurements in the experiments, a comparison of the base pressures in CFD can be made. Figure 4.7 shows the pressure distribution on the base of the vehicle for the open- and closed-cooling. In both cases, a different position of the high-pressure region in the numerical simulations can be seen in the number plate region and rear bumper, whereas in the wind-tunnel results the higher pressure region was located at the rear windscreen. Near the vehicle's shoulder around the rear lamp (sometimes referred to as catwalk) a vortex appears, which is not visible in the wind-tunnel surface pressures.

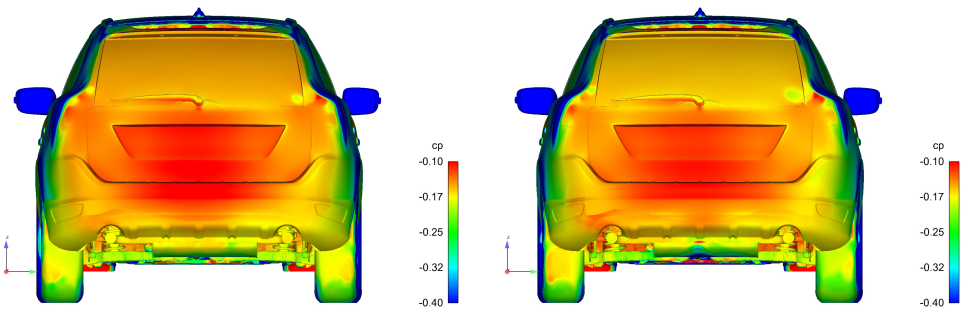

(a) (b)

Figure 4.7: *C_p on base of 4WD in CFD: (a) Open-cooling, (b) Closed-cooling.*

4.2.3 Wake measurements

This difference also had an impact on the wake shape behind the vehicle. For CFD, Figure 4.8 shows the wake in the transverse plane and horizontal plane. The transverse plane shows two low-drag regions from the underbody for the open-cooling configuration, similar to Figure 4.3a. Also the general shape was predicted well. Nevertheless differences can be noted in an enhanced wake from the side-mirrors and a more distinct vortex structure, originating from the A-pillar. In Figure 4.8b, the structural differences are larger in that the numerical simulations predict a *W-shaped* wake shape, whereas the experiments showed one single region. The wake width does not change much between the configurations, whereas the closed-cooling experiences a faster total pressure recovery further away from the vehicle's rear end.
Looking at the closure region predicted in CFD, it tends to be 0.3 m to 0.5 m shorter compared to the wind-tunnel test. However in the wind tunnel the pressure values measured by the probes are not corrected for blockage, giving a lower value. This lower value results in an over-predicted wake length.

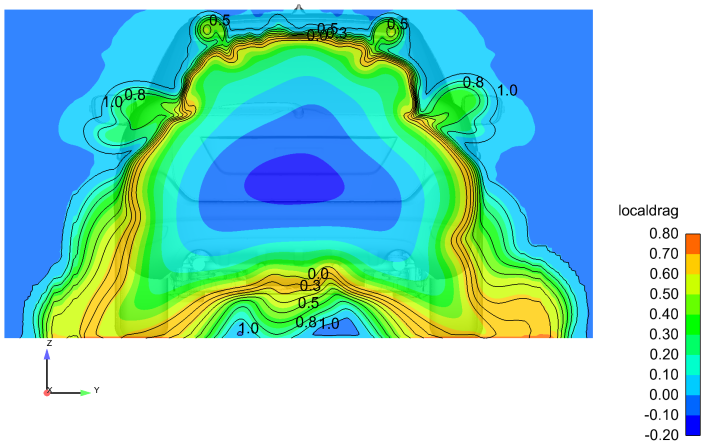

(a)

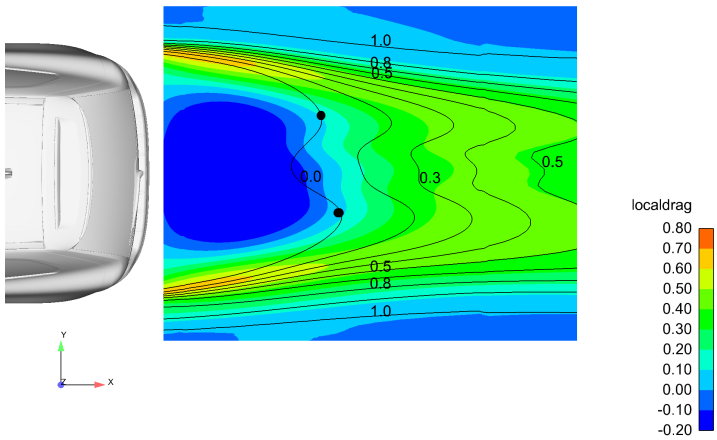

(b)

Figure 4.8: *Local drag superimposed with $c_{p_{tot}}$-contour lines in CFD: (a) Xplane, (b) Zplane. [52]*

An overall view at the wake shape in CFD is given in Figure 4.9 of an isosurface region where $c_{p_{tot}} = 0$, where a better representation of the closure region can be seen. Here, a closure region with three closure points can be observed.

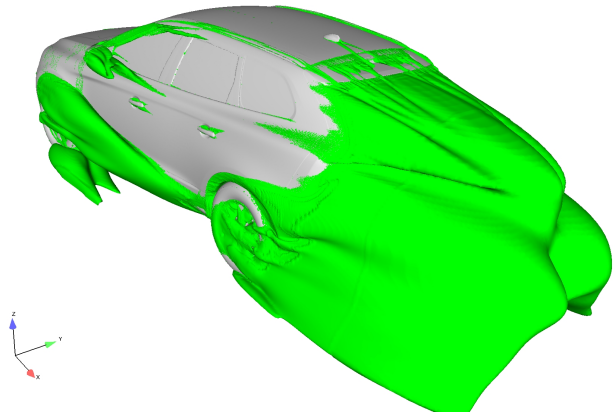

Figure 4.9: *Isosurface of* $c_{p_{tot}} = 0$.

4.2.4 Wake analysis plot

The result for the open- and closed-cooling configurations of the 4WD XC60 are given in Figure 4.10. The structures from the different geometrical regions are made visible in the figure by the vertical lines. These lines are placed symmetrical with respect to the 180° mark. The division starts with the flow from the roof at symmetry, which is 0°, whereas the 180° mark is the flow from the underbody at symmetry. The section between 0° and 180° corresponds to the wake from the left side of the vehicle following a counter-clockwise direction; the remaining is consequently the right side. The geometrical division based on the numbering system is: (1) roof region, (2) side-mirror region, (3) side region, (4) wheel region, and (5) underbody region.
The effect of the cooling drag can mostly be seen from the underbody flow. Its interaction with the wheel wake on the right side of the vehicle shifted to a lower θ-value (from 220° to 210°) and increased in relative local drag. On the left side the effect is less visible but still present. These narrow the wheel wakes, lowering the overall drag of the closed-cooling configuration.

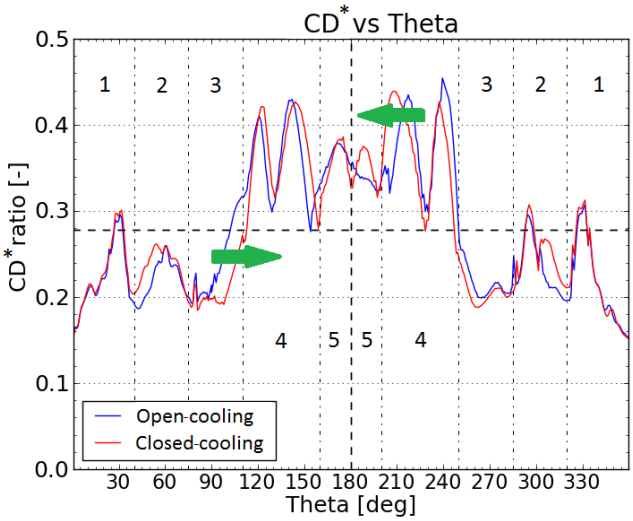

Figure 4.10: *Integrated local drag vs θ on polar mesh*

5 Conclusion

This research has investigated the surface pressures near the base and wake shape behind a Volvo XC60 for four configurations with a different drag coefficient. The number of configurations was sufficient enough to correlate a lower C_D to the most favourable wake shape.

Surface pressure measurements for open-cooling, closed-cooling and closed-front in the wind tunnel have shown a higher pressure region located at the rear wind screen. The overall pressure distribution is similar for the three configurations, but the pressure magnitude is more negative in the closed-cooling and closed-front cases compared to the open-cooling. However, the standard deviation of pressure in these configurations is higher.
The wake behind the open-cooling, closed-cooling and extended roof spoiler variants has also been studied. Its shape has been investigated through the use of three planes with extra focus for the shear layer and closure region. The closed-cooling and extended roof spoiler show an increased total pressure recovery in the flow coming from the roof further downstream of the vehicle. The closed-cooling accomplishes this by an improved lower wake flow from the underbody and simultaneously a reduced wake area. The extended roof spoiler achieves it by improving the pressure recovery over the roof. The spoiler reduces the wake size by having a more downward inclined shear layer.
When the force measurements from the wind tunnel balance were connected to the position of the traversing unit in the wake measurements, a change in drag coefficient compared to the reference case, when no traversing unit is present in the wake (traversing unit in parking position) could be observed.

Steady-state simulations of the three configurations show in general a good agreement with the experiments. The change in drag coefficient between the configurations is predicted well. Also, similarities in surface pressures and in wake shape with the experiments can be observed. Nevertheless, some distinct differences are present too. These are mostly visible on the surface in the location of the higher pressure region and in the wake through the transverse plane and horizontal plane.
The simulations predict the location of the closure point to be 0.3 to 0.5 m closer to the car's rear end compared to the experiments.

A new method for quantifying the contribution of different car regions to the overall drag has been presented. This technique has first been developed on simplified models, after which it has been tested on fully-detailed models, including the open- and closed cooling XC60 configurations.

6 Future work

Experimentally, a standalone PSI-system will first be developed to allow for a continuous acquisition of pressure data in the wind tunnel. Initially this methodology will give the possibility for the acquisition of unsteady measurement data on the base surface of passenger vehicles. But the system should also be able to measure unsteady wake pressures.
With the aid of this system, unsteady measurements will be taken to investigate the frequency and propagation of the different wake structures. A correlation of the wake structures, originating from different flow regions around the vehicle, will be made to look for structure interaction and an attempt will be made to link these structures to aerodynamic drag.

Numerically, an aerodynamic methodology for unsteady simulations will continue to be developed. This will give an alternative method to study the wake movement behind the car in time and in space.

With use of both the wind tunnel and CFD, conceptual changes to the base of the vehicle will be made with the purpose of reducing air resistance. These changes will then be investigated to understand how the wake structures affect the drag and stability of the vehicles.

Base pressure changes due to the presence of the traversing unit will be studied numerically as well as experimentally. To make the numerical simulations, a CAD model of the traversing unit was recently created.

The wake analysis method of quantifying the flow contribution from different geometric regions to the overall drag will be implemented in further configuration studies during this research. This will give additional insight in the potential of the technique and will help to translate the plots into meaningful alterations to the vehicle's geometry resulting in a wake balance.

References

[1] Enerdata. *Global Energy Statistical Yearbook 2012*. URL: `http://yearbook.enerdata.net` (visited on 2013-03-15).

[2] Association, International Energy. *Key World Energy Stats 2012* (2012).

[3] BP. *BP Statistical Review of World Energy 2012* (2012).

[4] Commission, European. URL: `http://ec.europa.eu/clima/policies/transport/vehicles/cars/index_en.htm` (visited on 2013-05-11).

[5] Eurostat, European Commision. URL: `http://epp.eurostat.ec.europa.eu/portal/page/portal/energy/introduction` (visited on 2013-05-11).

[6] BP. URL: `http://www.bp.com/statisticalreview` (visited on 2013-05-11).

[7] IEA, International Energy Association. *Statistical Review 2012*. URL: `http://www.iea.org/publications/freepublications/publication/name,32870,en.html` (visited on 2013-03-13).

[8] Hucho, W.H. *Road Vehicle Aerodynamics*. 4th edition. United States of America: Society of Automotive Engineers Inc., 1998.

[9] Barnard, R.H. *Road Vehicle Aerodynamic Design*. 2nd edition. England: Mechaero Publishing, 2001.

[10] Landstrom, C. *Passenger Car Wheel Aerodynamics*. Gothenburg, Sweden: Chalmers University of Technology, 2011.

[11] Elofsson, P. and Bannister, M. *Drag Reduction Mechanisms Due to Moving Ground and Wheel Rotation in Passenger Vehicles. SAE World Congress* 2002-01-0531 (2002).

[12] Wäschle, A. *The Influence of Rotating Wheels on Vehicle Aerodynamics - Numerical and Experimental Investigations. SAE World Congress* 2007-01-0107 (2007).

[13] Sapnaras, D. and Dimitriou, I. *Experimental Analysis of the Underbody Pressure Distribution of a Series Vehicle on the Road and in the Wind Tunnel. SAE World Congress* 2008-01-0802 (2008).

[14] Cooper, K.R., Bertenyi, T., Dutil, G., and Syms, J. *The Aerodynamic Performance of Automotive Underbody Diffusers. SAE International Congress and Exposition* 980030 (1998).

[15] D'Hondt, M., Gilliéron, P., and Devinant, P. *Experimental Investigation on the Flow Around a Simplified Geometry of Automotive Engine Compartment. Experiments in Fluids* 50 (2011), 1317–1334.

[16] Ohshima, T., Hamatani, K., Ninoyu, M., and Nakagawa, K. *Influence of the Cooling Air Flow Outlet on the Aerodynamic Characteristics. JSAE* 19 (1998), 137–142.

[17] Baeder, D., Indinger, T., Adams, N., and Decker, F. *Comparison of Numerical Simulations with Experiments of Bluff Bodies Including Under-Hood Flow. SAE World Congress* 2011-01-0171 (2011).

[18] Cogotti, A. *Flow-Field Surveys Behind Three Squareback Car Models Using a New "Fourteen-Hole" Probe. SAE International Congress and Exposition* 870243 (1987).

[19] Ahmed, S.R. and Baumert, W. *The Structures of Wake Flow Behind Road Vehicles. ASME_CSME Conference* (1979).

[20] Ahmed, S.R. *Wake Structure of Typical Automobile Shapes. ASME Conference* 103 (1981).

[21] Cogotti, A. *A Strategy for Optimum Surveys of Passenger Car-Flow Fields. SAE International Congress and Exposition* 890374 (1989).

[22] Morelli, A. *A New Aerodynamic Approach to Advanced Automobile Basic Shapes. SAE World Congress* 2000-01-0491 (2000).

[23] Duell, E.G. and George, A.R. *Experimental Study of a Ground Vehicle Body Unsteady Near Wake. SAE World Congress* 1999-01-0812 (1999).

[24] Sims-Williams, D.B. and Dominy, R.G. *The Reconstruction of Periodic Pressure Fields from Point Measurements. SAE World Congress* 1999-01-0809 (1999).

[25] Sims-Williams, D.B., Dominy, R.G., and Howell, J.P. *An Investigation into Large Scale Unsteady Structures in the Wake of Real and Idealized Hatchback Car Models. SAE World Congress* 2001-01-1041 (2001).

[26] Gilhome, B.R., Saunders, J.W., and Sheridan, J. *Time Average and Unsteady Near-Wake Analysis of Cars. SAE World Congress* 2001-01-1040 (2001).

[27] Song, J., Yoshioka, S., Kato, T., and Kohama, Y. *Characteristics of Flow Behind a Passenger Vehicle. SAE World Congress* 2001-01-1040 (2001).

[28] Schröck, D., Widdecke, N.., and Wiedemann, J. *The Effect of High Turbulence Intensities on Surface Pressure Fluctuations and Wake Structures of a Vehicle Models. SAE World Congress* 2009-01-0001 (2009).

[29] Al-Garni, A.M., Bernal, L.P., and Khalighi, B. *Experimental Investigation of the Near Wake of a Pick-up Truck. SAE World Congress* 2003-01-0651 (2003).

[30] Al-Garni, A.M., Bernal, L.P., and Khalighi, B. *Experimental Investigation of the Flow Around a Generic SUV. SAE World Congress* 2004-01-0228 (2004).

[31] Viswanath, P.R. *Flow Management Techniques for Base and Afterbody Drag Reduction. Progress Aerospace Science* 32 (1996), 79–129.

[32] Tanner, M. *Reduction of Base Drag. Progress Aerospace Science* 16 (1975), 369–384.

[33] Irving Brown, Y.A., Windsor, S., and Gaylard, A.P. *The Effect of Base Bleed and Rear Cavities on the Drag of an SUV. SAE World Congress* 2010-01-0512 (2010).

[34] Littlewood, R., Passmore, M., and Wood, D. *An Investigation into the Wake Structure of Square Back Vehicles and the Effect of Structure Modification on Resultant Vehicle Forces. SAE World Congress* 2011-37-0015 (2011).

[35] Barlow, J.B., Guterres, R., Ranzenbach, R., and Williams, J. *Wake Structures of Rectangular Bodies with Radiused Edges near a Plane Surface. SAE World Congress* 1999-01-0648 (1999).

[36] Barlow, J.B., Guterres, R., and Ranzenbach, R. *Rectangular Bodies with Radiused Edges in Ground Effect. 17th AIAA Applied Aerodynamics Conference* AIAA-99-3153 (1999).

[37] Perry, A-K. and Passmore, M. *The Impact of Underbody Roughness on Rear Wake Structures of a Squareback Vehicle. SAE World Congress* 2013-01-0463 (2013).

[38] Le Good, G.M. and Garry, K.P. *On the Use of Reference Models in Automotive Aerodynamics. SAE World Congress* 2004-01-1308 (2004).

[39] Heft, A.I., Indinger, T., and Adams, N.A. *Introduction of a New Realistic Generic Car Model for Aerodynamic Investigations. SAE World Congress* 2012-01-0168 (2012).

[40] Heft, A.I., Indinger, T., and Adams, N.A. *Experimental and Numerical Investigation of the DrivAer model. ASME Fluids Engineering Summer Meeting* FEDSM2012-72272 (2012).

[41] Strangfeld, C., Wieser, D., Schmidt, H-J., Woszidlo, R., Nayeri, C., and Paschereit, C. *Experimental Study of Baseline Flow Characteristics for the Realistic Car Model DrivAer. SAE World Congress* 2013-01-1251 (2013).

[42] Menter, F.R. *Best Practise: Scale-Resolving Simulations in ANSYS CFD.* ANSYS Germany GmbH. Apr. 2012.

[43] Sternéus, J., Walker, T., and Bender, T. *Upgrade of the Volvo Cars Aerodynamic Wind Tunnel. SAE World Congress* 2007-01-1043 (2007).

[44] Corporation, Aeroprobe. *Omniprobe.* URL: `http://www.aeroprobe.com/uploads/Omniprobe-for-web.pdf` (visited on 2013-05-10).

[45] Ramakrishnan, V. and Rediniotis, O.K. *Development of a 12-Hole Omnidirectional Flow-Velocity Measurement Probe. AIAA Journal* 45.6 (2007), 1430–1432.

[46] Pressure Systems, Inc. *PSI 8400 Data Acquisition System.* URL: `http://www.meas-spec.com/product/t_product.aspx?id=9313` (visited on 2013-05-10).

[47] Pressure Systems, Inc. *ESP-HD Pressure Scanners.* URL: `http://www.meas-spec.com/product/t_product.aspx?id=9311#` (visited on 2013-05-10).

[48] Sebben, S. and Mlinaric, P. *Investigation of the Influence of Tyre Deflection and Tyre Contact Patch on CFD Predictions of Aerodynamic Forces on a Passenger Car. 7th MIRA International Vehicle Aerodynamics Conference* (October 2008).

[49] Chronéer, Z. *The CFD Process for Aerodynamics at Volvo Cars using HARPOON-FLUENT. 3rd European Automotive CFD Conference* (2007).

[50] Ivanic, T. and Gilliéron, P. "Aerodynamic drag and ways to reduce it". *Lecture Series VKI Institute.* Brussels: VKI Institute, 2005.

[51] Sterken, L., Sebben, S., and Löfdahl, L. *Alternative Approach in Ground Vehicle Wake Analysis. World Academy of Science, Engineering and Technology* 68 (2012).

[52] Sterken, L., Sebben, S., Walker, T., and Löfdahl, L. *Experimental and Numerical Investigations of the Base Wake on an SUV. SAE World Congress* 2013-01-0464 (2013).